ORIGINAL PAPER

Anatomy of mining-induced fault slip and a triggered rockburst

Cai-Ping Lu [1,2] · Bin Liu [3] · Biao Liu [1] · Yang Liu [1] · Hong-Yu Wang [4] · Heng Zhang [1]

Abstract

Fault slips and triggered rockbursts pose a significant threat to the safety of mining personnel and infrastructure in deep coal mines. Sudden and dynamic slip may occur along a pre-existing fault characterized by the presence of contact between two opposite faces. Such slips are capable of changing the balance of forces when mining activity is conducted in the area surrounding the fault at depth and are accompanied by energy release that has the potential to cause serious damage to roadways and working faces. The aim of the comprehensive investigation reported here was to elucidate the evolution of the stress field surrounding a fault due to mining activity in adjacent working faces, using Fast Lagrangian Analysis of Continua in 3 Dimensions (FLAC3D) numerical simulations, especially variations the high shear stress area. We then proposed the mining-induced fault slip mechanism. The evolution rule of sources during fault slip could be clearly explained using field microseism (MS) monitoring data, and the correlation between source parameters (e.g., static stress drop, peak particle velocity, and displacement) and fault slip was established. Correspondingly, the multi-parameter precursors of a rockburst induced by the fault slip were analyzed and summarized in detail. This work provides a number of reference points to be used for the warning and controlling of rockbursts triggered by fault slip in coal mines.

Keywords Fault slip · Stress field · Rockbursts · Microseism monitoring · Precursors

Introduction

Rockbursts in coal rock in deep coal mines are dynamic phenomena generally induced by changes in the stress regime associated with mining activity at deep levels. At the present time, rockbursts cannot be precisely predicted or effectively prevented using available techniques (Schmidt 2013). Such was the case of the disastrous rockburst that occurred in the 21201 working face of the Qianqiu coal mine (QCM) on

June 5, 2008, resulting in serious damage to a 630-m-long roadway, including closure of a 105-m-long section, ejection of 3975 t of coal, and desorption of 1700 m^3 gas with a peak concentration of up to 8.1%. As of 2016, the number of statistically enumerated rockbursts in coal mines in China was 167. This hazard represents an increasing threat to miners and underground infrastructure.

Rockbursts can be classified into two categories: strain rockbursts (strainburst) and fault-slip rockbursts (Ortlepp 1992; Wong 1992). The former occurs when localized high stress concentrations are produced and develop adjacent to a working face or excavation boundaries, causing brittle failure of the intact coal or rock, generally with ejected materials of less than 100 t (Blake and Hedley 2003). Strain rockbursts usually occur in specific areas characterized by a concentration of original high stress that can be verified in advance; thus, this type of rockburst is relatively easy to predict and prevent compared with fault-slip rockbursts. Fault-slip rockbursts, on the other hand, occur when excavation activities alter the stresses acting on a fault, ultimately triggering sudden slip behavior along the fault plane. This type of rockburst is not usually restricted to the proximity of an advancing working face, but rather arises in an area of hundreds of meters surrounding the working face (McKinnon 2006).

✉ Cai-Ping Lu
cplucumt@126.com

1   Key Laboratory of Deep Coal Resource Mining (Ministry of Education), School of Mines, China University of Mining and Technology, Xuzhou, Jiangsu 221116, People's Republic of China

2   Department of Civil Engineering and Lassonde Institute, University of Toronto, Toronto, Ontario M5S 1A4, Canada

3   Institute of Rock and Soil Mechanics, Chinese Academy of sciences, Wuhan, Hubei 430071, People's Republic of China

4   Department of Civil, Environmental and Mining Engineering, School of Engineering, University of Western Australia, Crawley, WA 6009, Australia

Fault-induced rockburst is universally considered to be a key safety issue in deep coal mines. Due to heterogeneous nature of the fault, the slip of the fault plane and fracture of intact parts significantly contribute to the difficulty of predicting such rockbursts.

A better understanding of mining-induced fault slips and subsequent rockburst precursors subjected to stress changes by excavation is very important. To elucidate the fault-slip mechanism, a number of triaxial tests and field observations have been conducted to understand fault-slip mechanics, including the characteristics of frictional strength, slip and failure criteria, and energy accumulation and release on the fault during slip (Moore et al. 1990; Williams et al. 1992; Urbancic et al. 1993; Blanpied et al. 1995; Savage et al. 1996; Ortlepp 2000; Sprenke et al. 2002; Goebel et al. 2012; Paige et al. 2013; Mclaskey and Lockner 2016). Analysis of the triaxial, biaxial, and ring-shear configurations have been also widely carried out to investigate the shear characteristics of artificial faults (Summers and Byerlee 1977; Dieterich 1981; Shimamoto and Tsutsumi 1994; Beeler et al. 1996; Faulkner et al. 2010; Ikari and Saffer 2011; Niemeijer et al. 2011), with particular focus on the double-direct experiments of fault stick-slip (Karner and Marone 1998; Mair et al. 2007; Beeler et al. 2014). Recently, some methods for alleviating fault-slip rockbursts have been put forward and implemented in coal mines, including reducing the volume of excavations, avoiding man-made high stress concentrations (Sjöberg et al. 2012), using microseism (MS) monitoring to provide early warning (Malek et al. 2008), and using de-stress blasting to release the accumulated strain energy (Yao et al. 2009; Lu et al. 2018). Board et al. (1992) proposed an interesting method to reduce the friction coefficient, namely, the injection of pressurized fluid into a fault plane to pre-induce low-energy slip events with a small recurrence interval, thereby mitigating the danger of large-energy slip events occurring unexpectedly.

Initiating pre-emptive fluid- or de-stress-triggered slips of faults is one strategy to potentially prevent rockbursts by possibly reducing the potential shear stress that may contribute to unpredictable slip events (Kaiser et al. 2013). However, if the excavation areas adjacent to a fault are in a high-stress concentration state, even a small-energy fault slip may trigger a rockburst. Therefore, it is crucial to be able to accurately delineate high stress concentrations in advance and even identify the precursors of slip, with the aim to warn and/or mitigate the danger of fault-induced rockbursts. Unfortunately, gaining knowledge of the triggering mechanism between stress changes adjacent to a fault and subsequent slips remains a challenge. Especially enigmatic is the link between fault slip and MS monitoring, which is a key issue in being able to accurately warn for rockbursts.

The aim of the work reported here was to investigate the role that changes in mining-induced stress play in the effectiveness of fault slip and the associated rockburst hazard. We have investigated this topic using two approaches: a series of numerical simulations and in-situ integrated observations, including MS monitoring, electromagnetic emission (EME), and gas emission. Based on a rockburst induced by a field-scale fault slip, we analyzed and summarized the multi-parameter precursors. Based on this analysis, we were able to clearly explain the triggering mechanism of fault slip in response to changes in shear stress due to sequential excavation.

Site conditions

Geological settings of the 25110 working face

A fully mechanized top-coal caving mining technique is used to mine the 25110 working face, located in the right wing of the #25 mining area of the Yuejing coal mine (YCM). To the north are the 25090, 25070, 25050, 25030, and 25010 working faces, from bottom to top, respectively. The 25110 working face is adjacent to the F16 thrust-reverse fault in the southeast direction and to down-dip gateway pillars of the #23 and #25 mining areas in the east and west directions, respectively. The buried depth of the 25110 working face is approximately 1000 m, the slope is 192 m, and the lengths of the headentry and tailentry are 856 and 878 m, respectively. The #2-1 coal seam has a thickness of 7.6–13.2 m. It was identified to have strong rockburst tendency and to be composed of three to five sandy mudstone layers that have a total thickness of 2.1 m and a single-layer thickness ranging from 0 to 0.9 m; the inclination ranges from 12.5° to 15.4°, with an average inclination of 13°. The immediate floor is composed of 20-m-thick mudstone; the false roof consists of 0.2-m-thick sandy mudstone partly intruded by hard quartz sandstone; the immediate roof is composed of 18-m-thick mudstone; and the primary roof is mainly sandstone and conglomerate. The headentry adopts the bolt–mesh–anchor system combined with 36 U "O- type" shed and gate-type hydraulic support. Figure 1 shows the planar sketch of the right wing of the #25 mining area and the F16 fault.

Tectonic parameters of the F16 fault

The large thrusts are probably weak faults. The slip occurs on all of the thrust surfaces simultaneously, whereas evidence from earthquakes suggests that thrusts operate by the overall accumulation of displacement on slip patches located on different parts of the fault at different times (Price 1988). The F16 reverse-thrust fault was formed under huge compaction and the overthrusting effect of the thrust-nappe tectonic system. The fault extends approximately 45 km along a nearly EW strike, with dip angles of 75° and 15–35° in the shallow and deep parts, respectively. The throw of the F16 fault is 50–

Fig. 1 Planar sketch of the right wing of the #25 mining areact and the F16 fault
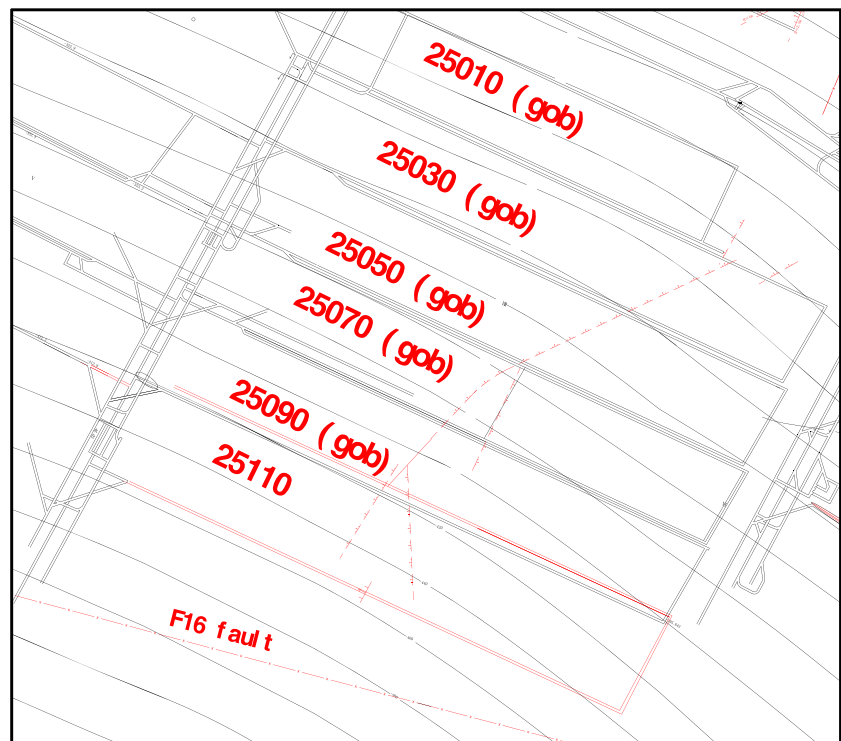
500 m, and the horizontal separation is 120–1080 m. The fault activation could be easily triggered due to the weakness of the thrust property and disturbance by mining activity at the neighboring 25110 working face.

Mining-induced slip of the F16 fault and a triggering rockburst

MS characteristics during the F16 fault slip

MS system

An Engineering Seismology Group (ESG) system was installed and implemented on September 29, 2008 at YCM with the aim to monitor the F16 fault slip and provide a warning of rockburst. The ESG system consists of three main components, namely, the geophones, the Paladin digital signal acquisition system, and the Hyperion digital signal processing system, as well as of minor parts. The frequency response, sampling rate, and transmission speed of the geophone are 0.01–100 MHz, 50–10 kHz, and 200 MB/s, respectively. The resolution of the system is 14-bit digital with a signal acquisition capability of up to 125 MHz, and the geophones use acceleration sensors. To minimize the location error of the source, pre-blasting was implemented to calibrate the velocity model for locating; the locating error of the system was found to be generally less than 10 m when the P-wave velocity was set to 4000 m/s.

The headentry of the 25110 working face is close to the F16 fault, and the tailentry is located below the lower sublayer of the adjacent 25090 working face that is characterized by a de-stressed zone. Therefore, the geophones of the MS system were mainly arranged in the headentry to monitor F16 fault activity, and the layout of the geophones was updated regularly with advances in the 25110 working face. A total of 23 geophones were installed in underground roadways, of which four and three were arranged in the headentry and tailentry, respectively.

Source locations during the F16 fault slip

A sudden drop in shear stress will accompany the slip of a fault, with the strain energy being released seismically. Otherwise, the slip will be gradual, continuous, and aseismic without an obvious release of energy, as no excess shear stress is permitted to build up and drive episodic slip behavior. Therefore, each MS event will be produced when one slip of a fault occurs, and the location and energy of the source can be calculated by the MS monitoring system. Figure 2 shows the vertical profile chart of the MS sources located in the surroundings of the 25110 working face and the F16 fault during the driving and initial mining periods (July 2009 to October 2010).

The spatial–temporal distribution of the sources with vertical depth of − 300 to − 500 m is shown clearly in Fig. 2. Most of the sources are symmetrically distributed on the upper and lower plates of the F16 fault; in particular, a large number of

Fig. 2 Profile chart of the MS sources located in the surroundings of the 25110 working face and the F16 fault
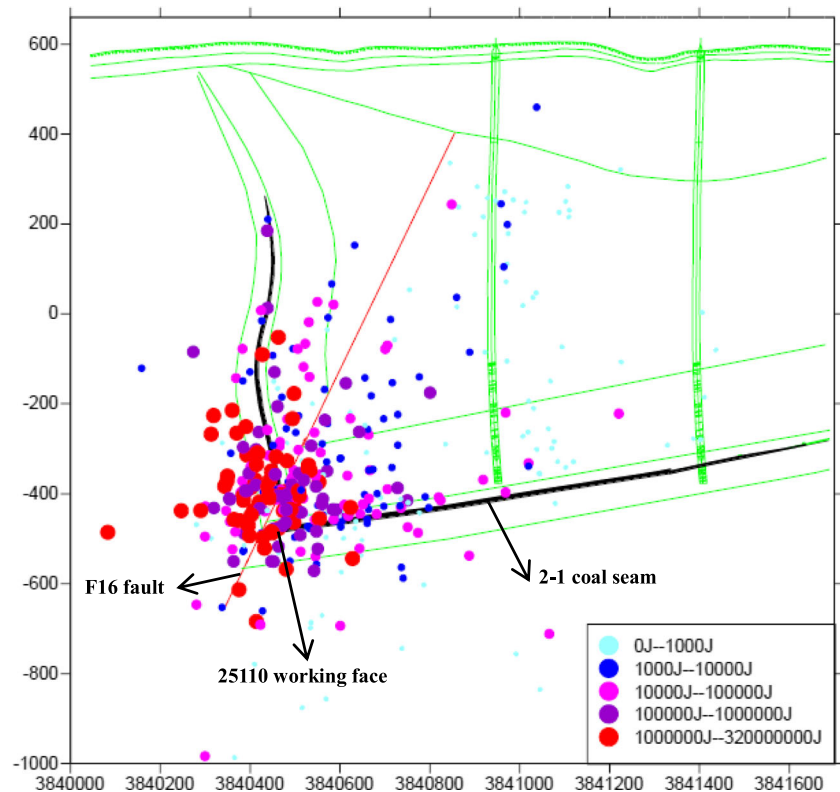
high-energy sources are clustered around the fault surface. Many high-energy sources are also concentrated in the surroundings of the 25110 working face due to mining activity. During the initial excavation period from July 2009 to March 2010, the source energy was relatively lower due to only weak disturbance as the spacing distance between the driving head and the F16 fault was large. The source energy subsequently increased rapidly until October 2010 during the late driving and initial mining period. When the 25110 working face gradually approached the F16 fault during the initial excavation period, the mining-induced disturbance significantly strengthened. It was expected that once the shear stress reached or surpassed the shear strength of the F16 fault due to the decrease in normal stress caused by mining activity, the slip would inevitably be triggered. Thus, the concentration of the high-energy sources surrounding the F16 fault was closely associated with the slips.

The planar distributions of the sources during driving and the initial mining periods of the 25110 working face were studied to further reveal the slip and associated energy release of the F16 fault, as shown in Fig. 3.

In Fig. 3a, many small-energy sources ($E < 10^3$ J) generated during driving can be seen to be vertically distributed in the shallow part of the F16 fault at some distance from the 25110 working face. In comparison, almost all of the high-energy sources ($E > 10^5$ J) are clustered in the area surrounding the F16 fault area closest to the 25110 working face, demonstrating that the subsequent excavation caused the

fault slip and the accumulated energy release. Due to small variations in the in-situ stress field with roadway driving, the slip of the F16 fault was negligible and, therefore, the releasing energy was also low.

It can be seen from Fig. 3b that at the initial mining stage of the 25110 working face, the total number of MS events was clearly lower than that shown in Fig. 3a; however, the source energy was generally higher, and most of the events were larger than 10^6 J. In particular, some high-energy sources emerged in the F16 fault area at some distance from the 25110 working face, indicating that the mining activity caused large-scale deformation and fracture of the surrounding coal-rock and a corresponding reduction and transfer of the original stress. Therefore, it can be inferred that the normal stress of the F16 fault near the 25110 working face was obviously reduced and that the friction on the fault plane was also correspondingly decreased. Because the shear stress reached or surpassed the shear strength of the F16 fault in the mining-influenced zone, the triggering of the slip was inevitably accompanied by a release of high energy.

Slips of the F16 fault

In order to further reveal the mining-induced slip characteristics of the F16 fault, we selected three distinct slips that occurred on July 23 and 25 and August 5, 2010, respectively, to analyze the correlation between the energy, static stress drop,

Fig. 3 Planar distributions of the sources during the driving (**a**) and initial mining periods (**b**) of the 25110 working face
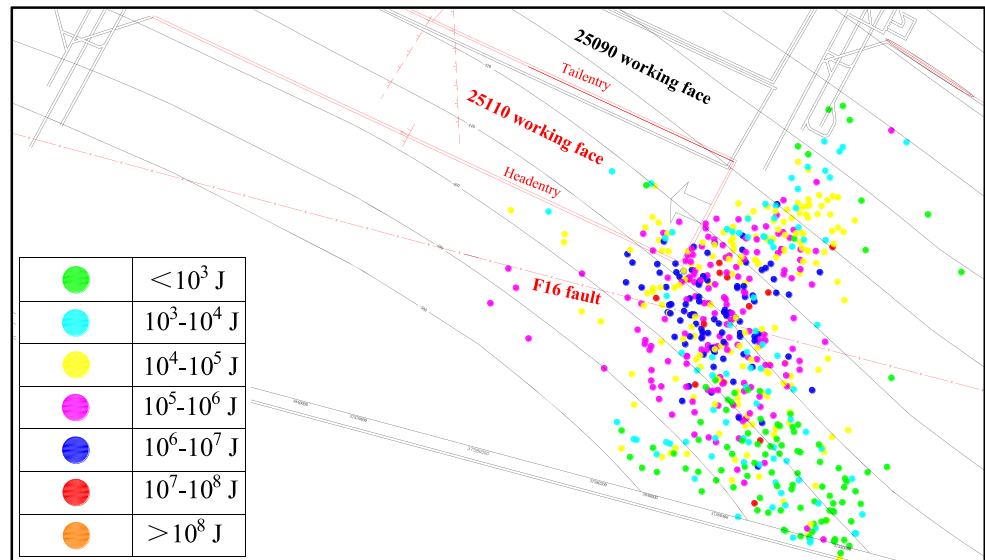
(a) Sources location during driving from April 27, 2009 to July 18, 2010
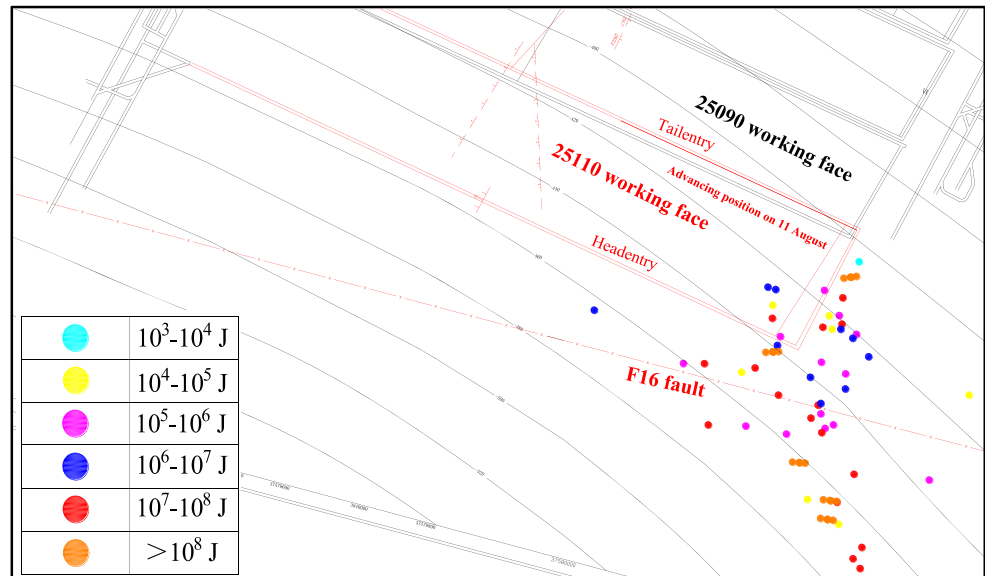
(b) Sources location during initial mining from July 19 to August 13, 2010

S-wave/P-wave energy (E_S/E_P), peak particle velocity (PPV), and maximum displacement of each slip, as shown in Fig. 4.

As seen in Fig. 4, the static stress drop, PPV, and maximum displacement rose continuously with the increasing energy of each slip, whereas the E_S/E_P showed a slight decrease initially, which was folllowed by a sharp rise, demonstrating that the shear activity was weaker on July 25 than on August 5. The static stress drop is generally not dependent on the scale of the fault and usually ranges between 0.1–10 MPa for natural earthquakes (Zoback and Gorelick 2012). However, the stress drops occurring over localized asperities or stronger portions of fault surfaces may be significantly higher than the general range and, for example, they can reach 70 MPa in some cases (McGarr

et al. 1979). Therefore, the stress drops observed on July 25 and August 5 were within the expected range, while the stress drop on July 23 reached up to 100 MPa, which may be the result of failure of portions of the F16 fault surface with higher strength. The slip that occurred on July 23 triggered a rockburst that appeared in the range of 820–830 m in the headentry of the 25110 working face; the maximum displacement reached 0.24 m, and the PPV was up to 21.2 m/s. In addition, an MS event is closely associated with shear failure along geological discontinuity when $E_S/E_P > 10$ (Boatwright and Fletcher 1984). All of the E_S/E_P values of the three slips were larger than 20, demonstrating that the events were significantly characterized by shear failure in nature of the F16 fault.

Fig. 4 Correlation between
energy, static stress drop, E_S/E_P,
PPV, and maximum displacement
of each slip

Fig. 4 Correlation between energy, static stress drop, E_S/E_P, PPV, and maximum displacement of each slip
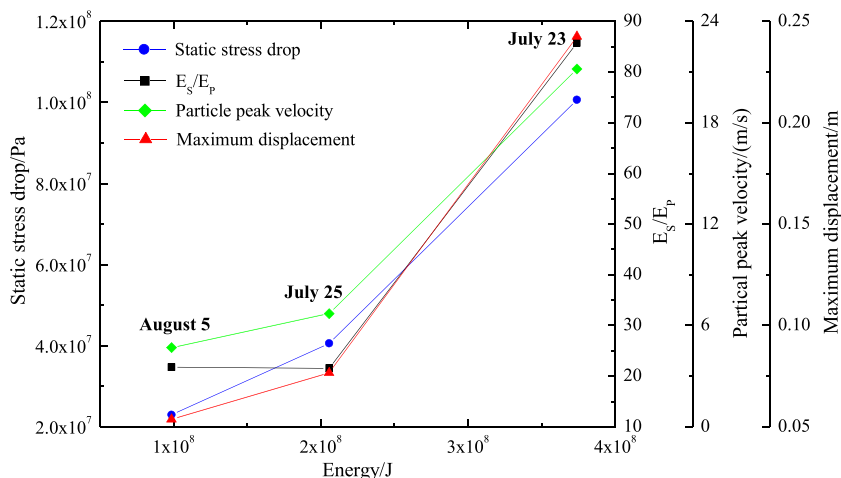
Stress distribution characteristics surrounding the F16 fault during excavation

Mining-induced fault slip is due to stress redistribution in response to excavation during the advancing of roadways and working faces. On adversely oriented faults, excavation can cause both an increase in shear stress, τ, and a reduction in normal stress, σ_n (Blake and Hedley 2003). If this trend reaches the point where the induced shear stress exceeds the shear strength of the fault, the fault will inevitably slip.

In this case, the excavation disturbance can reduce the effective normal stress acting on a critically stressed fault until it slips in accordance with the Mohr–Coulomb criterion:

$$\tau \geq (\sigma_n - p_m)\tan\varphi + c \tag{1}$$

where τ and σ_n represent the shear and normal stresses acting on the fault, respectively, p_m is the stress relief on the fault caused by excavation, φ is the friction angle of the fault surface, and c is the corresponding cohesion.

A critically stressed fault may be present where the shear stress contributing to drive the slip is slightly smaller than the shear strength of the fault, due to partially to normal stress clamping the fault. When excavation occurs through or near the fault, in the absence of the lower strata completely "holding" the fault structure, the initial normal stress σ_n will be reduced to some extent by the stress relief, p_m. Continuous excavation may also lead to a subsequent increase in τ. Both factors contribute to the fault slip. Thus, the analysis of stress acting on the fault is crucial for verification of the slip trend.

Modeling

Since it is difficult to record stress variation in real time, numerical simulation is a feasible method at the present stage. A numerical model was built using Fast Lagrangian Analysis of Continua in 3 Dimensions (FLAC3D) numerical modeling software (Itasca Consulting Group, Itasca International, Inc.,

Minneapolis, MN, USA) to investigate the effect of excavation of the 25110 working face on stress variation of the F16 fault. To reduce the computational costs, the geological conditions of the models were appropriately simplified. Vertically, from bottom to top, the model consisted of sandstone, mudstone, 2-1 coal seam, mudstone, sandy mudstone, and conglomerate. The size of the model was 1365 m (length) × 1050 m (width) × 350 m (height) and included a total of 267,936 elements; in particular, local elements in the excavation area were refined. The 'Interface' function of the FLAC3D software can simulate the structural planes, such as faults and discontinuities in coal and rock.

The bottom boundary of the model was fixed, and the three-dimensional stress regime was loaded by the horizontal x-axis σ_x of − 20.5 MPa, the horizontal y-axis σ_y of − 20.5 MPa, and the vertical z-axis σ_z of − 20.5 MPa on the top boundary. The mechanical parameters of coal and rock of the model, based on geological surveys and laboratory test results, are shown in Table 1.

Static stress distribution surrounding the F16 fault

Stress distribution of the profile where $y = 500$ m The profile of the model was made along the direction of $y = 500$ m, and the corresponding stress distribution is shown in Fig. 5.

It can be seen from Fig. 5a that the normal stress of the left and right sides of the area was larger than that in the middle and that the normal stress manifested discontinuous distribution on the upper and lower plates near the F16 fault. The normal stress maximum at the top of the upper plate of the F16 fault was approximately 22 MPa, and the minimum normal stress was approximately 6 MPa at the bottom of lower plate. The shear stress on the upper and lower plates evolved differently (Fig. 5b), with the latter gradually decreasing to the minimum of 6 MPa with increasing depth, while the former was higher with a maximum of 17 MPa. From Fig. 5c, it is evident that the vertical stress increased with increasing depth, with the minimum vertical stress of about 14 MPa located at the top of the upper plate of the F16 fault,

Table 1 Mechanical parameters of coal and rock of the model

Mineral	UCS (MPa)	Elastic modulus (GPa)	Poisson's ratio	Cohesion/ (MPa)	Internal frictional angle (°)	Density (kg/m³)
Conglomerate	52.05	42.16	0.2	29	40	2600
Sandy mudstone	35.25	26.88	0.15	24.7	35	2600
Mudstone	20.00	4	0.35	6	28	2500
2-1 coal sean	14.43	2	0.4	1.68	25	1350
Mudstone	20.00	4	0.35	6	28	2500
Sandstone	67.33	48.19	0.2	31	42	2700

UCS, Uniaxial compressive strength

and the maximum vertical stress of approximately 38 MPa located at the bottom of the upper plate. In addition, the maximum principal stress was basically consistent with the vertical stress, and the minimum principal stress also corresponded to the normal stress, indicating that both normal and shear stresses on the lower plate of the F16 fault at depth were small.
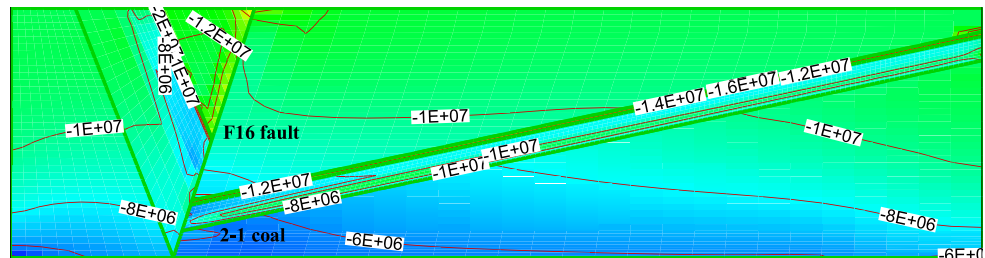
Stress distribution along the 2-1 coal inclination The profile of the model was made along the 2-1 coal inclination, and the corresponding stress distribution is shown in Fig. 6. It can be seen from this figure that the horizontal stress in the 2-1 coal

seam showed slight fluctuations but remained at about 9 MPa. The horizontal y-directional stress in the 2-1 coal seam was basically similar to the horizontal x-directional stress, and the value remained at about 10 MPa (Fig. 6b). The variation in vertical stress near the lower plate of the F16 fault in the middle of the 2-1 coal seam was different from that of horizontal stress, first appearing as a gradient rise from right to left and then as a gradient reduction as it with approached the F16 fault due to the influence of the lower plate (Fig. 6c). In addition, the stress variation on the upper plate differed from that on the lower
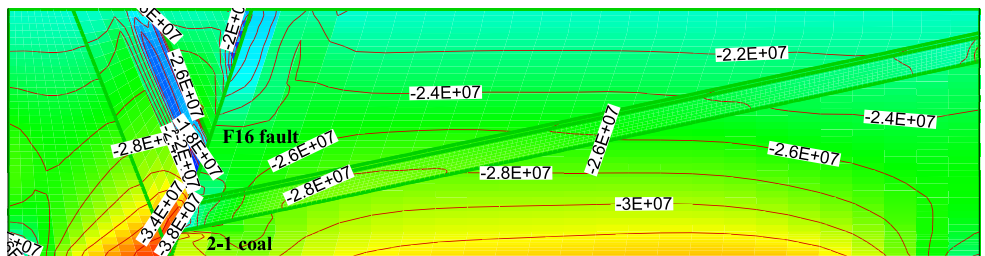
Fig. 5 **a**–**c** Stress distribution of the profile where $y = 500$ m
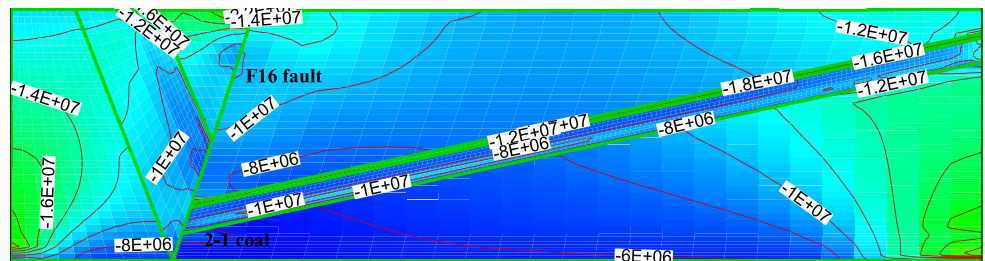
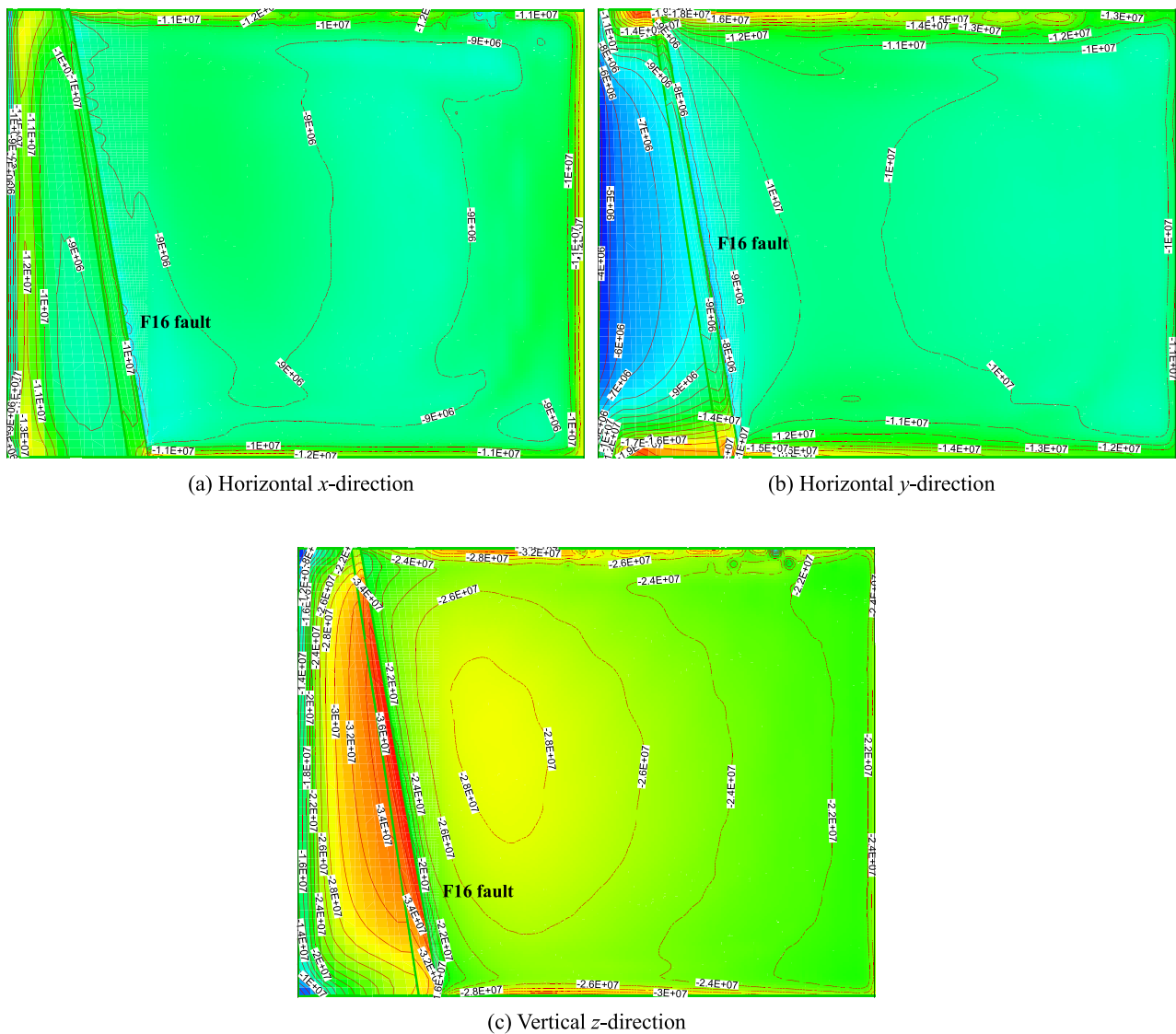(a) Horizontal x-directional normal stress

(b) Horizontal y-directional shear stress

(c) Vertical z-directional stress

(a) Horizontal *x*-direction

(b) Horizontal *y*-direction

(c) Vertical *z*-direction

Fig. 6 **a**–**c** Stress distribution along the 2-1 coal inclination. Note: the right side of the F16 fault is the lower plate

plate, and the former was obviously higher than the latter, indicating that the fault caused discontinuous distribution of the stress across the upper and lower plates. The maximum and minimum principal stresses were approximately consistent with the vertical and horizontal stresses, respectively.

In summary, there was a discontinuous stress distribution near the upper and lower plates of the F16 fault, and the gradient increasing trend of vertical stress along the 2-1 coal seam inclination from shallow to deep was removed by the F16 fault. Approaching the fault, the gradient reduction of vertical stress appeared to be due to the influence of the lower plate.

Variation in mining-induced shear stress on the F16 fault

The shear stress distribution along the 2-1 coal dip before and after excavation of the 25090 working face was analyzed to reveal the slip mechanism of the F16 fault, as shown in Fig. 7.

The original shear stress in the 25110 working face located at lower plate of the F16 fault was clearly different before and after the excavation, as seen in Fig. 7. The shear stress in this area was positive at approximately 1 MPa before the excavation, and then became negative at about 6 MPa after excavation of the 25090 working face. This change may have caused the slip of the lower plate of the F16 fault and aggravated the rockburst risk of the 25110 working face.

During excavation of the 25110 working face, the shear stress along the 2-1 coal dip was simulated at 20-m intervals. The results of this simulation show that there were no obvious changes in shear stress before and after excavation, but there were significant changes in the high shear stress zone (high shear stress refers to a value of > 6 MPa), as shown in Fig. 8.

In Fig. 8, the difference in the high shear stress zone before and after excavation gradually increased with advancing distances of 20 to 180 m, except for a sudden drop due to the first
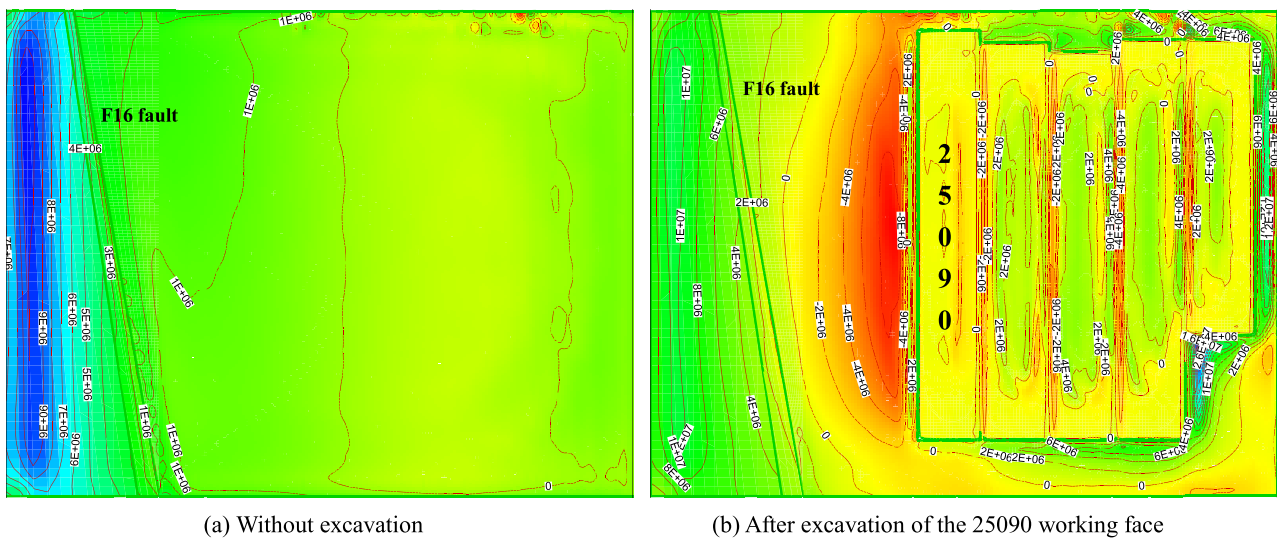
(a) Without excavation   (b) After excavation of the 25090 working face

Fig. 7 Shear stress profile along the 2-1 coal dip. **a** Without excavation, **b** after excavation

roof cave-in at the advancing distance of 40 m. When the roof experienced the square cave-in at the advancing distance of 180 m, the difference reached its maximum and then dropped suddenly. The distance to the F16 fault gradually increased with advancing of the 25110 working face, while the difference decreased continuously, indicating that the high shear stress near the 25110 working face easily triggered the slip of the F16 fault at the initial mining stage combined with normal stress reduction. With gradual increases in the distance to the fault with the advancing of the 25110 working face, the high shear stress zone was reduced and, therefore, the F16 fault was relatively difficult to slip.

A faulting-induced rockburst and multi-parameter precursors

A disastrous rockburst with a magnitude of M_L 2.7 occurred in the headentry of the 25110 working face on August 11, 2010, and the released energy reached up to 9×10^7 J. By August 11,

the advancing distances of the tailentry and headentry of the 25110 working face were 17.1 m and 31.2 m, respectively. The deformation and destruction were significant in the headentry 340 m ahead of the cut, and the O-type shed and gate-type hydraulic supports were seriously damaged. In particular, the #3, #4, and #5 water injection drill sites in the headentry at 528, 704, and 795 m ahead of the cut were completely closed. The rockburst also caused pronounced floor heave and cross-section reduction of the roadways, with the maximum floor heave reaching 2.3 m. The shock wave generated by the rockburst stirred up a cloud of coal dust in the headentry and tailentry. The deformation and destruction of the headentry after the rockburst are shown in Fig. 9.

The #9, #10, #12, and #19 geophones were arranged around the 25110 working face. The MS waveforms of the rockburst recorded by the four geophones are shown in Fig. 10. The waveforms manifested a long duration for the four geophones located on the lower plate of the F16 fault; the first-motion amplitude of the P wave was smaller, and the

Fig. 8 Variation in the high shear stress zone with advancing of the 25110 working face
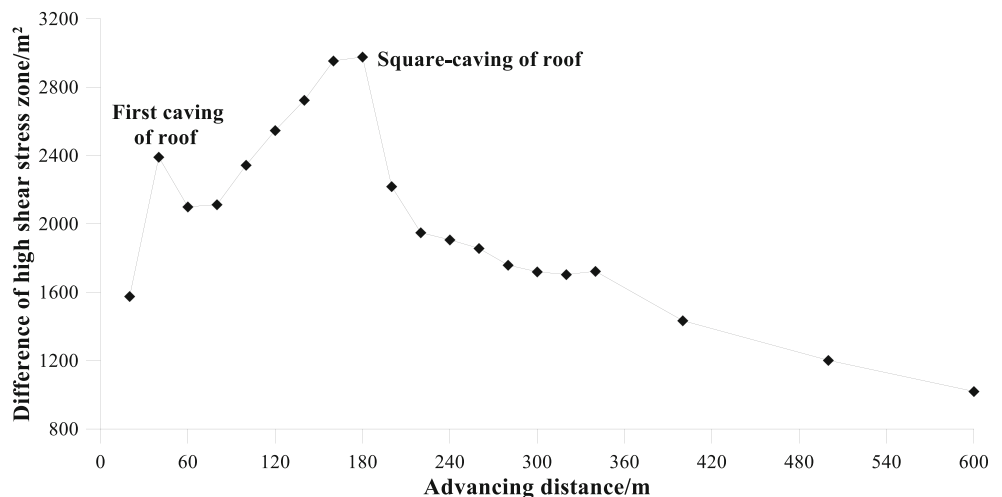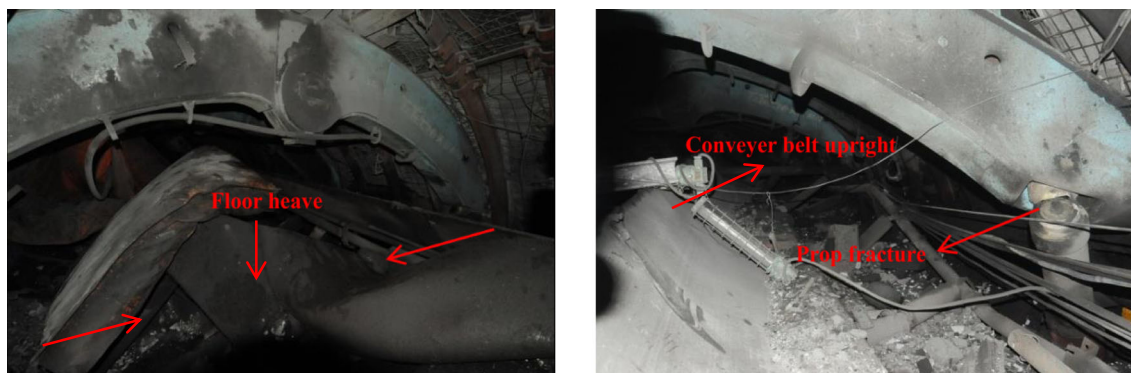
(a) Shear-induced floor heave   (b) Conveyer belt upright and shear-induced prop fracture

Fig. 9 Photographs of the deformation (**a**) of the headway and destruction of equipment (**b**) of the headentry of the 25100 working face caused by the rockburst on August 11, 2010

first-motion direction was upward. Based on the spatial orientation between the F16 fault plane and the four geophones, it can be verified that the MS signals were closely associated with the slip of the F16 fault.

Macroscopic precursors of the rockburst

The EME may reflect the stress of the headentry of the 25110 working face based on the relationship between EME and stress (Yamada et al. 1989; Frid et al. 1992). For field monitoring, the antenna of the KBD5 EME portable apparatus is commonly fixed and the receiving end is oriented vertically towards the middle–upper part of the coal wall within 5 m. The amplitude and pulse indexes and their variations in EME generated by coal and rock deformation and failure are measured by a non-contacted method to warn of the risk of rockburst. The interval between two adjacent monitoring points is normally 20 m. In our study, we arranged five monitoring points each in the tailentry and headentry 80 m ahead of the 25110 working face, and the average amplitude was
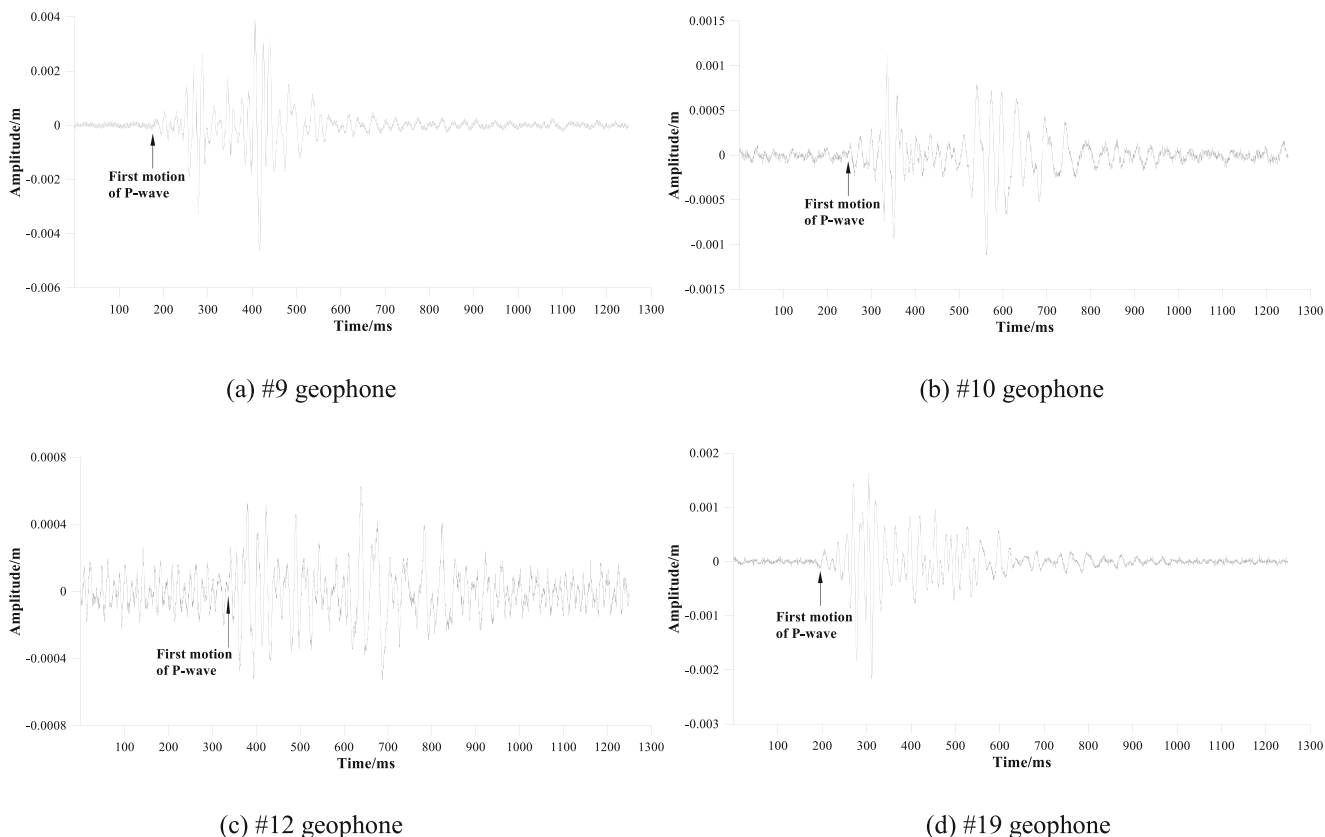
(a) #9 geophone

(b) #10 geophone

(c) #12 geophone

(d) #19 geophone

Fig. 10 MS waveforms of the rockburst recorded by the #9, #10, #12, and #19 geophones

calculated as the result of that day. In addition, the average resistance of all hydraulic supports was also correspondingly calculated to verify the stress status of the 25110 working face combined with EME. Variations in both EME amplitude and support resistance from July 18 to August 11, 2010 (Fig. 11).

Comprehensive analysis of EME amplitude and support resistance shown in Fig. 11 revealed that both showed a gradually decreasing trend from July 18 to August 9 and then suddenly dropped to the minimum value on August 10—following which the rockburst occurred. Therefore, it can be extrapolated that micro-cracks in the overlying roof strata experienced sequentially initiation, growth, and interaction with mining activity of the 25110 working face accompanied with a gradual decrease of stress. When the roof cave-in occurred, the normal stress near the F16 fault suddenly dropped. Together, these data indicate that the shear stress near the F16 fault did not show an obvious change, whereas the normal stress was significantly reduced, thus inevitably triggering the slip of the F16 fault. In summary, the reduction in normal stress reflected by EME amplitude and support resistance can be regarded as one of the key warning factors of a fault slip.

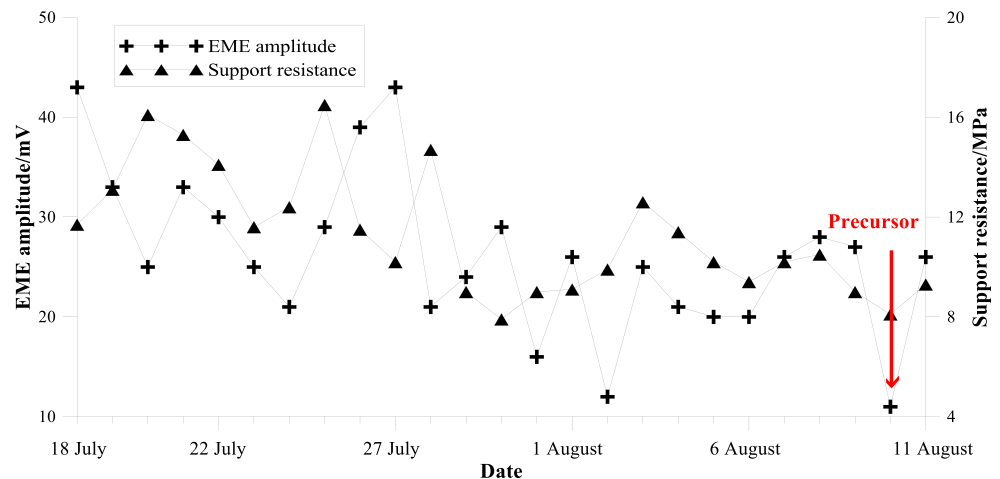## MS frequency-spectrum evolution before and after the rockburst

There is an abundance of laboratory and field evidence showing that a switch occurs from a dominantly hybrid type of MS to a dominantly low-frequency type of MS when a rockburst is imminent (Spetzler et al. 1987; Read et al. 1995; Benson et al. 2010; He et al. 2010). In particular, the MS resonance frequency has been shown to decrease in experiments monitoring roof falls using displacement, stress, and MS monitoring prior to the final roof fall (Shen et al. 2008). The evolution of the frequency-spectrum of the MS events located near the F16 fault, as recorded by three geophones closest to the fault, including three events prior to the rockburst and two events after the rockburst, are shown in Fig. 12 .

The frequency-spectrum distributions shown on Fig. 12 are characterized by low amplitude, wide spectrum, and high central frequency before the rockburst, indicating that the F16 fault began to generate micro-slip due to disturbance of the 25110 working face caused by mining activities, accompanied with a small energy release. Prior to the rockburst at 18:07:28, the amplitude spectra increased suddenly, indicating that the large slip of the F16 fault was triggered when both the normal stress and shear strength of the fault decreased and the shear stress reached or exceeded the critical value of shear strength due to mining-induced relief effect of the 25110 working face. Simultaneously, a large amount of energy was released, and eventually the rockburst was triggered. With the initiation, growth, and interaction of micro-fissures along the F16 fault plane into macro-fractures after the rockburst, the amplitude spectra generated by the fault slip increased suddenly, accompanied by an obvious reduction of the dominant frequencies, clearly demonstrating the large slip of the fault. Thereafter, the amplitude spectra fell with the gradual stability of the fault, while the dominant frequencies significantly increased to a high-frequency band. Therefore, the evolution from dominantly hybrid to dominantly low-frequency type combined with the increasing amplitude can be regarded as a convincing precursor of a fault slip.

Abnormal gas emission during the rockburst

The dynamic load generated by a fault slip will result in a sudden rupture of coal and rock in the critical stress condition by means of propagation and attenuation of the shock wave, producing fissures that both contribute to the development of gas outburst channels and accelerate the escape velocity of the gas to trigger gas outbursts. For coal-containing gas, the abnormally high emission due to a high gas pressure and a high stress concentration may be an effective precursor of a rockburst. In the Rhine-Westphal coal field, Hawusike coal field, and Ruhr coal field in Germany, many rockbursts have been accompanied by abnormal gas emissions (Hu et al. 2008).

Fig. 11 Variations in both electromagnetic emission (*EME*) amplitude and support resistance from July 18 to August 11, 2010

(a) #9 geophone

(b) #10 geophone

(c) #12 geophone
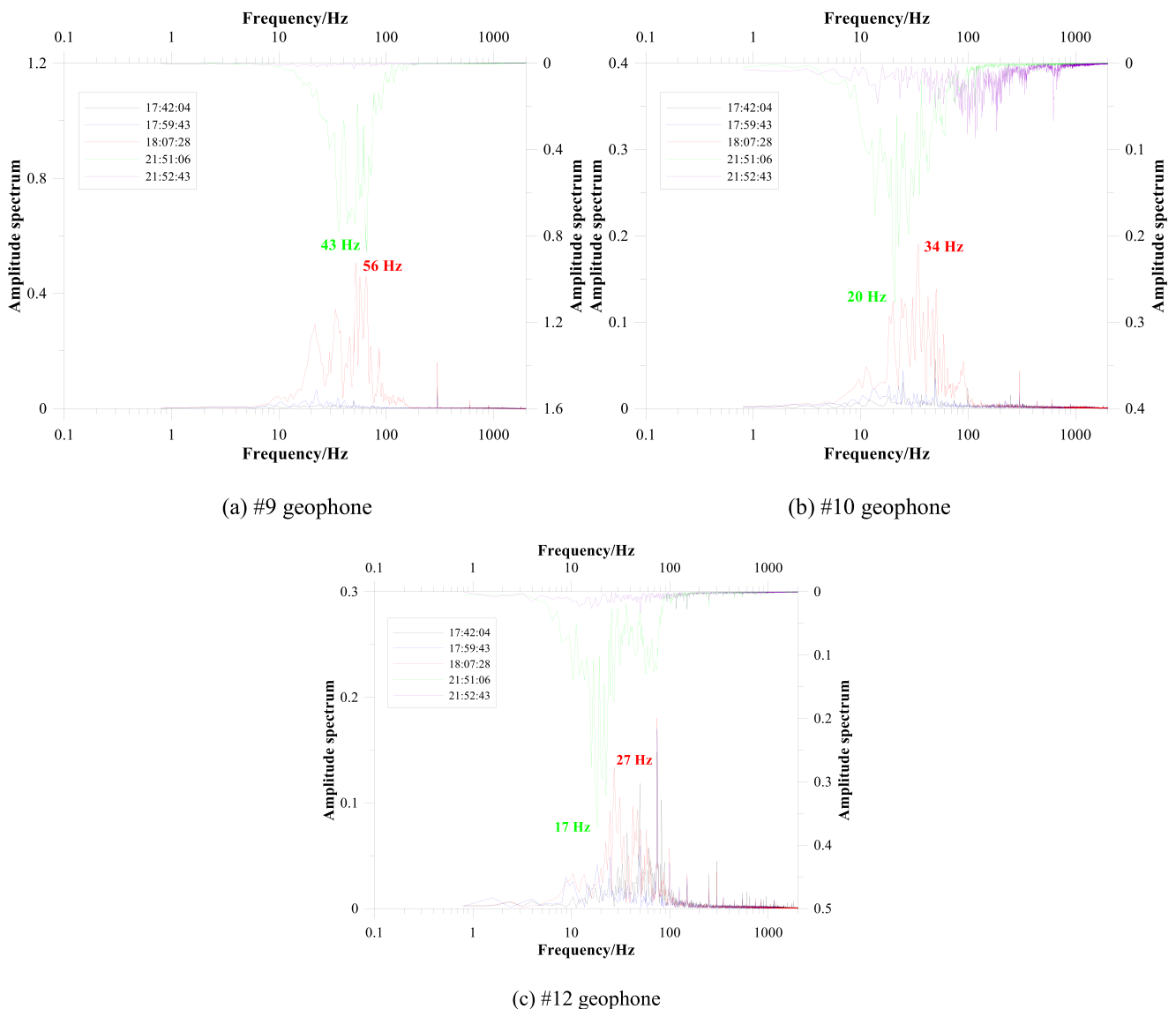
Fig. 12 Frequency-spectrum evolution of the MS events located near the F16 fault before and after the rockburst. Note: the occurrence time of the rockburst was 18:11:53 on August 11
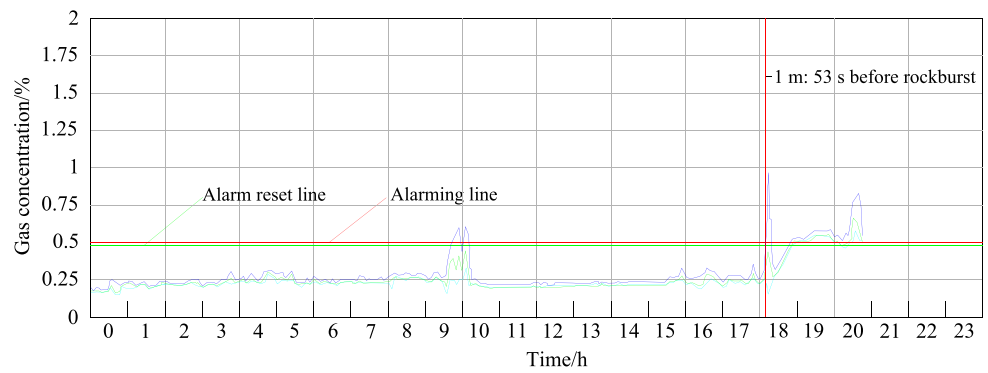
The variations in gas concentration at the upper corner of the 25110 working face and the #3 water injection drill onsite were continuously recorded during the rockburst, as shown in Fig. 13.

It can be seen from Fig. 13a that the gas concentration at the upper corner of the 25110 working face increased abruptly at approximately 9:00 a.m. on August 11 and that the maximum value exceeded the alarming line, indicating that the abnormal gas emission from coal and rock was possibly associated with micro-slip of the F16 fault. Thereafter, the gas concentration dropped sharply to below the critical value (alarming value). In particular, the gas concentration began to show significantly continuous fluctuations during the 2-h period prior to the rockburst, which can be regarded as a precursor of obvious slip of the F16 fault causing the fracture of coal and rock. It is worth noting that the concentration began to rise sharply from 1 min and 53 s before the rockburst, reaching a maximum when the rockburst occurred,

followed first by a sudden drop and a gradual increase to above the alarming line where it remained; this trend indicates the continuous gas outburst from the fractured coal and rock after the rockburst. In Fig. 13b, the gas concentration at the #3 water injection drill onsite is initially not apparent, and then it began to appear at about 6 h before the rockburst, once again verifying the micro-slip process of the F16 fault. The concentration sharply rose after the rockburst, with the maximum exceeding 2%, followed by sudden drop, with the value remaining above the alarming line.

When a fault slides, the seismic waves with a large amount of energy are produced and propagate in all directions. The residual energy after attenuation will transmit and superimpose on surrounding coal and rock combined with the original static stress, and part of the residual energy transforms to the kinetic energy of the gas absorbed in the coal and rock. This significantly strengthens the activity of the gas, and the

Fig. 13 Variations in gas concentration at the upper corner of the 25110 working face (**a**) and the #3 water injection drill onsite (**b**) during the rockburst. Note: (1) The blue, green, and cyan lines represent the maximum, average, and minimum values of the recorded gas concentration. (2) The gas concentration at the upper corner (**a**) increased by 0.1–0.2% compared with before the rockburst. (3) The gas concentration suddenly increased to 2% in **b** owing to complete closure of the #3 water injection drill onsite after the rockburst. (4) The gas gushed out from the water injection hole in the headentry 770 m ahead of the cut, and the concentration exceeded 10%

(a) Gas concentration at the upper corner
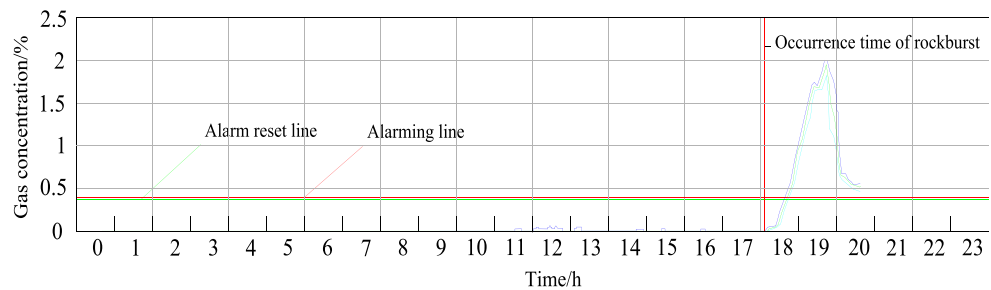
(b) Gas concentration at the #3 water injection drill onsite

vibration of coal and rock is triggered due to the interference of seismic wave generated by the fault slip. In addition, the gas temperature rises, exacerbating the desorption and escaping velocity and promoting the formation of the macro-fractures serving as channels that contribute to accelerating gas emission. Thus, the continuous fluctuations of the gas concentration near a fault can be regarded as a precursor of the fault slip.

Conclusions

(1) When driving and mining gradually approach the F16 fault, both normal stress and friction force on the fault plane were reduced. Once shear stress reaches or exceeds shear strength of the fault, the fault slip will occur with significant energy release. In addition, the driving operation weakly disturbs the stress field near the fault, and the energy of the MS sources clustering in the fault area near the 25110 working surface is low. However, the mining activity easily causes obvious slip of the fault, and the energy of the MS sources is higher accompanied with obvious stress drop.

(2) The static stress drop, PPV, and maximum displacement rise with the increasing energy released by the fault slip. However, the E_S/E_P first show a slight decrease and then dramatic increase.

(3) The variation in shear stress is not obvious before and after excavation of the 25110 working face, whereas the high shear stress zone changes significantly, indicating that the high shear stress zone is capable of triggering the F16 fault slip at the initial mining stage accompanied with the decrease in normal stress.

(4) The MS manifests low amplitude, a wide spectrum, and a high central frequency before the rockburst, and the amplitude suddenly rises prior to the rockburst, indicating obvious slip of the F16 fault accompanied by a large amount of energy release and obvious reduction of dominant frequency. Thereafter, the MS amplitude drops with gradual stability of the fault, and the dominant frequency moves to the high-frequency band. In addition, the continuous fluctuation of gas concentration can also be regarded as a precursor of fault slip.

References

Beeler NM, Tullis TE, Blanpied ML, Weeks JD (1996) Frictional behavior of large displacement experimental faults. J Geophys Res 101: 8697–8715

Beeler NM, Tullis TE, Junger J, Kilgore B, Goldsby D (2014) Laboratory constraints on models of earthquake recurrence. J Geophys Res 119: 8770–8791

Benson PM, Vinciguerra S, Meredith PG, Young PR (2010) Spatio-temporal evolution of volcano seismicity: a laboratory study. Earth Planet Sci Lett 297:315–323

Blake W, Hedley DGF (2003) Rockbursts: case studies from north American hard-rock mines. Society for Mining, Metallurgy, and Exploration, Inc., Littleton

Blanpied ML, Lockner DA, Byerlee JD (1995) Frictional slip of granite at hydrothermal conditions. J Geophys Res 100:13045–13064

Board M, Rorke T, Williams G, Gay N (1992) Fluid injection for rockburst control in deep mining. Tillerson JR & Wawersik WR (Eds.) Proceedings of the 33rd U.S. Symposium on Rock Mechanics. A. A. Balkema, Rotterdam, pp 111–120

Boatwright J, Fletcher JB (1984) The partition of radiated energy between P and S waves. Bull Seismol Soc Am 74:361–376

Dieterich J (1981) Constitutive properties of faults with simulated gouge D.C. In: Carter NL et al. (Eds.) Mechanical behavior of crustal rocks. Geophys Monogr Ser 24:102–120

Faulkner D, Jackson C, Lunn R, Schlische R, Shipton Z, Wibberly C (2010) A review of recent developments concerning the structure, mechanics and fluid flow properties of fault zones. J Struct Geol 32:1557–1575

Frid V, Shabarov A, Proskurjakov V (1992) Formation of electromagnetic radiation in coal stratum. J Min Sci 28:139–145

Goebel THW, Becker TW, Schorlemmer D, Stanchits S, Sammis C, Rybacki E, Dresen G (2012) Identifying fault heterogeneity through mapping spatial anomalies in acoustic emission statistics. J Geophys Res Solid Earth 117:1–18

He MC, Miao JL, Feng JL (2010) Rock burst process of limestone and its acoustic emission characteristics under true-triaxial unloading conditions. Int J Rock Mech Min Sci 47:286–298

Hu QT, Zhou SN, Zhou XQ (2008) Mechanical mechanism of coal and gas outburst process. J China Coal Soc 33:1368–1372

Ikari M, Saffer D (2011) Comparison of frictional strength and velocity dependence between fault zones in the Nankai accretionary complex. Geochem Geophys Geosyst 12:239–241

Kaiser PK, Valley B, Dusseault MB, Duff D (2013) Hydraulic fracturing mine back trials—design rationale and project status. Jeffrey R, Bunger AP, McLennan J (Eds.) Effective and sustainable hydraulic fracturing. IntechOpen, London, pp 877–890

Karner SL, Marone C (1998) The effect of shear load on frictional healing in simulated fault gouge. Geophys Res Lett 25:4561–4564

Lu CP, Liu Y, Zhang N, Zhao TB, Wang HY (2018) In-situ and experimental investigations of rockburst precursor and prevention induced by fault slip. Int J Rock Mech Min Sci 108:86–95

Mair M, Marone C, Young RP (2007) Rate dependence of acoustic emissions generated during shear of simulated fault gouge. Bull Seismol Soc Am 97:1841–1849

Malek F, Trifu C, Suorineni FT, Espley S, Yao M (2008) Management of high stress and seismicity at Vale Inco Creighton Mine. Amadei B, Kranz RL, Scott GA, Smeallie PH (Eds.) Proceedings of the 42nd U.S. Rock Mechanics Symposium. American Rock Mechanics Association, Alexandria, pp 8

McGarr A, Spottiswoode SM, Gay NC, Ortlepp WD (1979) Observations relevant to seismic driving stress, stress drop, and efficiency. J Geophys Res Solid Earth 84:2251–2261

McKinnon SD (2006) Triggering of seismicity remote from active mining excavations. Rock Mech Rock Eng 39:255–279

Mclaskey GC, Lockner DA (2016) Calibrated acoustic emission system records M −3.5 to M −8 events generated on a saw-cut granite sample. Rock Mech Rock Eng 49:4527–4536

Moore DE, Summers R, Byerlee JD (1990) Deformation of granite during triaxial friction tests. Rossmanith HP (Ed) Proceedings of the International Conference on Mechanics of Jointed and Faulted Rock, A. A. Balkema, Rotterdam, pp 345–352

Niemeijer A, Toro DG, Nielsen S, Felice FD (2011) Frictional melting of gabbro under extreme experimental conditions of normal stress, acceleration and sliding velocity. J Geophys Res 116:117–130

Ortlepp W (1992) Note on fault-slip motion inferred from a study of micro-cataclastic particles from an underground shear rupture. Pure Appl Geophys 139:677–695

Ortlepp WD (2000) Observation of mining-induced faults in an intact rock mass at depth. Int J Rock Mech Min Sci 37:423–436

Paige ES, Laurent G, Stephen DM (2013) The role of geologic structure and stress in triggering remote seismicity in Creighton Mine, Sudbury, Canada. Int J Rock Mech Min Sci 58:166–179

Price RA (1988) The mechanical paradox of large overthrusts. Geol Soc Am Bull 100:1898–1908

Read MD, Ayling MR, Meredith PG, Murrell SAF (1995) Microcracking during triaxial deformation of porous rocks monitored by changes in rock physical properties, II. Pore volumometry and acoustic emission measurements on water-saturated rocks. Tectonophysics 245: 223–235

Savage JC, Lockner DA, Byerlee JD (1996) Failure in laboratory fault models in triaxial tests. J Geophys Res 101:22215–22224

Schmidt ES (2018) Experimental and numerical investigation of hydraulic simulation as a risk mitigation technique for fault slip rockburst hazards in deep underground mining [Master thesis]. The University of British Columbia, Vancouver

Shen B, King A, Guo H (2008) Displacement, stress and seismicity in roadway roofs during mining-induced failure. Int J Rock Mech Min Sci 45:672–688

Shimamoto T, Tsutsumi A (1994) A new rotary-shear high-speed frictional testing machine: its basic design and scope of research. J Tecton Res Group Jpn 39:65–78 (in Japanese with English abstract)

Sjöberg J, Perman F, Quinteiro C, Malmgren L, Dahnér-Lindkvist C, Boskovic M (2012) Numerical analysis of alternative mining sequences to minimise potential for fault slip rockbursting. Min Technol 121:226–235

Spetzler H, Sondergeld C, Sobolev G, Salov B (1987) Seismic and strain studies on large laboratory rock samples being stressed to failure. Tectonophysics 1444:55–68

Sprenke F, White BG, Rohay AC, Whyatt JK, Stickney MC (2002) Comparison of body-wave displacement with damage observations of a rockburst, Coeur d'Alene mining district, Idaho Kenneth. Bull Seismol Soc Am 92:3321–3328

Summers R, Byerlee J (1977) A note on the effect of fault gouge composition on the stability of frictional sliding. Int J Rock Mech Min Sci 14:155–160

Urbancic TI, Trifu C, Young RP (1993) Microseismicity derived fault-planes and their relationship to focal mechanism, stress inversion, and geologic data. Geophys Res Lett 20:2475–2478

Williams TJ, Wideman CJ, Scott DF (1992) Case history of a slip-type rockburst. Pure Appl Geophys 139:627–637

Wong IG (1992) Recent developments in rockburst and mine seismicity research. Tillerson JR & Wawersik WR (Eds.) Proceedings of the 33rd U.S. Symposium on Rock Mechanics. A. A. Balkema, Rotterdam, pp 1103–1108

Yamada I, Masuda K, Mizutani H (1989) Electromagnetic and acoustic emission associated with rock fracture. Phys Earth Planet Inter 57: 157–168

Yao M, Chinnasane DR, Harding D (2009) Mitigation plans for mining in highly burst-prone ground conditions at Vale Inco Copper Cliff North Mine. Diederichs M & Grasselli G (Eds.) Proceedings of the 3rd CANUS Rock Mechanics Symposium. A. A. Balkema, Toronto, pp 1–11

Zoback MD, Gorelick SM (2012) Earthquake triggering and large-scale geologic storage of carbon dioxide. Proc Natl Acad Sci 109:10164–10168